Applied Catalysis B: Environmental 158–159 (2014) 418–425

Contents lists available at ScienceDirect

Applied Catalysis B: Environmental

journal homepage: www.elsevier.com/locate/apcatb

New insights into intermediate-temperature solid oxide fuel cells with oxygen-ion conducting electrolyte act as a catalyst for NO decomposition

Yun-Fei Bu[a,*], Dong Ding[b], Lu Gan[a], Xun-Hui Xiong[b], Wei Cai[a], Wen-Yi Tan[c], Qin Zhong[a,*]

[a] School of Chemical Engineering, Nanjing University of Science and Technology, Nanjing 210094, PR China
[b] Materials Science and Engineering, Georgia Institute of Technology, J. Erskine Love Bldg. 771 Ferst Drive, Atlanta, GA 30332-0245, USA
[c] Department of Environment Engineering, Nanjing Institute of Technology, Nanjing 211167, PR China

ARTICLE INFO

Article history:
Received 3 November 2013
Received in revised form 8 April 2014
Accepted 23 April 2014
Available online 2 May 2014

Keywords:
NO decomposition
Solid oxide fuel cells
Impedance
Perovskite
Cathode composite

ABSTRACT

The environmental problems and supply of clean and economical energy is grand global challenges. Direct decomposition of nitrogen oxides (NO_x) is the most ideal and effective approach for NO_x removal by catalysis, which has the great potential to alleviate the air pollution. On the other hand, solid oxide fuel cells (SOFCs) are one of the cleanest, most efficient chemical-to-electrical energy conversion systems. Here we reported a new electrochemical system to combine the traditional catalyst for direct decomposition of NO_x with an electric generation process through a SOFC. By nano-sized $La_{0.4}Ba_{0.6}Mn_{0.8}Mg_{0.2}O_{3-\delta}$ (LBMM), an effective catalyst widely used for NO_x decomposition, adopting an anode-support SOFC configuration, which consisted with the conventional NiO-samarium doped ceria (SDC) anode, and thin film SDC electrolyte, we demonstrated that complete decomposition of NO_x and a peak power density of 25 mW cm^{-2} at 600 °C when Ar containing 5% NO and 5% O_2 was fed to the cathode and 10% H_2 was used the fuel. The effect of the ratio between NO and O_2 was found to be critical for the NO conversion and SOFC performance. The dependence of temperature and gas composition on NO conversion was also investigated.

1. Introduction

Many environmental problems can be caused by nitrogen oxides (NO_x), such as acid rain, smog, and ozone depletion [1]. Therefore, great focus is on detecting and removing NO_x. Catalytic NO_x reduction processes such as NO_x storage reduction (NSR) system for lean-burn engines, the three-way catalyst device for gasoline-fueled vehicles [2,3], the electrochemical reduction of NO in solid–state electrochemical cell based on an oxygen ion conductor (electrochemical deNO_x) for lean-burn engines or gasoline-fueled vehicles [4], and selective catalytic reduction with ammonia (SCR) for large-scale combustion facilities have been developed so far [5,6]. Other effective deNO_x methods such as selective catalytic oxidation (SCO) [7], photochemical catalysis [8,9], microbial removal have also been sought [10]. The pros and cons of those methods are still under discussion now. For these deNO_x strategies, direct decomposition of NO and electrochemical reduction of NO are expected to be most desirable because of the quite simple process with high atom economy [11,12].

The directly decomposition of NO into N_2 and O_2 is the most ideal reaction for NO_x removal. Some catalysts, such like La_2O_3, Ba/MgO, and $BaMnO_3$ based perovskite oxides, are active toward the direct decomposition of NO [13,14]. The perovskite-type oxides exhibit catalytic activities in the high-temperature region from 500 to 850 °C, and are sustainable over long-term operation at the high temperatures required for NO decomposition [15,16]. Effects of dopant in $BaMnO_3$ perovskite oxide on the NO direct decomposition activity were investigated by Ishihara [17]. According to their research the highest N_2 yield was achieved by the use of $La_{0.2}Ba_{0.8}Mn_{0.8}Mg_{0.2}O_3$ [18]. The NO decomposition activity was greatly elevated by doping La and Mg for Ba and Mn site in $BaMnO_3$, respectively. The doping brings the oxygen vacancy sites, and also made it has some ability about fast electron transfer, high oxygen mobility and facile oxygen desorption, which is very significant property for NO decompositon. Recently, Ce and MgO have received

* Corresponding authors. Tel.: +86 25 84315517; fax: +86 25 84315517.
E-mail addresses: jpu441@yahoo.com (Y.-F. Bu), Zq304@mail.njust.edu.cn (Q. Zhong).

http://dx.doi.org/10.1016/j.apcatb.2014.04.041
0926-3373/

much attention in the designing of catalysts [19–21]. They were added simultaneously to La–Sr–Ni–O catalyst and got a substantial enhancement of activity for NO decomposition by Yang and his fellows. CeO_2 is often thought to participate in catalytic reaction acting as oxygen storing/scavenging component, to stabilize the dispersion of catalytic metals, and to decrease the apparent activation energy of catalyst, while MgO is a suitable material for adsorbing NO and for oxygen (O^-) mobilization, which facilitates NO decomposition reaction to occur. However, it is well known that on all materials, the NO decomposition is inhibited by added oxygen, the oxygen formed adsorbs also strongly on the catalyst, resulting in deactivation of the catalyst. That due to the reaction mechanism of NO decomposition over perovskite type oxides. A pair of NO molecules adsorbed on adjacent oxide ion vacancies at the surface interacts, while the two neighboring N—O bonds dissociate to produce a free N_2 molecule, which is released into the gas phase [22]. The existence of oxygen would inevitably compete and occupy the oxygen vacancy sites. In particular, the reaction temperature is high, high activity of NO decomposition is expected on perovskite oxides. Although increasing the reaction temperature is expected to decrease the negative effects of water and sulfur compounds. Advantages for reduced operating temperatures are considered to be longer life time and reduced costs of the total system.

The removal of NO by electrochemical reduction of NO in an all solid state cell is an alternative route as suggested by Pancharatnam et al. [23]. The reduction is undertaken by the electrons supplied to the cell during operation making the addition of reducing agents unnecessary. However, the main problem with this technique is the simultaneously reduction of oxygen at the cathode leading to a high current consumption [24]. So in the investigation of suitable electrode materials for electrochemical deNO_x a major challenge is to find electrode materials that have a sufficiently high activity and selectivity which are capable of reducing NO_x but not O_2, as reduction of O_2 is a competing reaction on the cathode. Perovskites oxides have been extensively investigated as the electrode for electrochemical deNO_x. The perovskite-type structure of oxides adopting expands the possibility of function design, because the original ions at both the A and B-sites can be replaced by other ions with similar ionic size and valence, while maintaining the original structure. The properties of substitution is to enhance the commercial utility of the perovskite devise by improving or fine tuning physical properties such as thermal stability, chemical stability, catalytic activity and electrolyte compatibility.

It is demonstrated that solid oxide fuel cells (SOFC) can convert the chemical energy of flexible fuel into electrical energy with high efficiency and environment benefits. It's a chemical reactor where the reaction takes place separately in two different chambers separated by a solid membrane. They operate at elevated temperature (300–1000 °C) to ensure adequate ionic conduction in the electrolyte. Moreover, simultaneous NO reduction and power generation have been shown to be feasible via the SOFCs. However, limited reports are available and they are normally focused on the traditional cathode materials of SOFC, which have activity for the oxygen reduction reaction but poor decomposition capability to NO [25–27]. For example, V_2O_5 or Cu added $La_{0.58}Sr_{0.4}Co_{0.2}Fe_{0.8}O_{3-\delta}$-GDC, and Cu-added $La_{0.8}Sr_{0.2}MnO_{3-\delta}$-GDC as the cathode reported by huang group, the high performance of the current–voltage can be getting at the temperature of 800 °C. Meanwhile, lowering the operating temperature of SOFCs to around 600–800 °C (intermediate-temperature SOFCs, IT-SOFCs) is one of the main goals in current SOFC research. The associated benefits include reducing the difficulties associated with sealing and thermal degradation, allowing the use of low-cost metallic interconnectors and suppressing reactions between the cell components. Thus, an IT-SOFCs coupled with NO decomposition could be very promising to accelerate the commercialization of SOFC technology while maximizing the NO decomposition. Fig. 1 illustrates the operating principles for a SOFC system serving as both power generation and NO decomposition. It is a typical SOFC single cell consists of three main components, i.e., a porous cathode and anode, sandwiching a dense electrolyte. The cathode functions as electrocatalyst for reduction of NO (or O_2 or both) into oxide ions. And the oxide ions diffuse through the solid–oxide electrolyte to the anode, where they electrochemically oxidize the fuel. The released electrons flow through an external circuit to the cathode to complete the circuit.

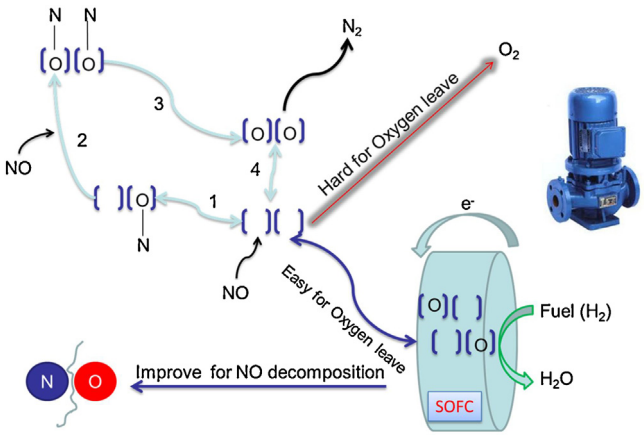

Fig. 1. Schematic view of the cooperation decomposition of NO by SOFC.

Some novelty perovskite-type materials have been reported as great promise in the application in NO decomposition [22], electrochemical deNO_x, and NO decomposition by oxygen transporting membrane [28,29]. In this study, La, Mg co-doping $BaMnO_3$ was used as our cathode materials. Since $La_{0.2}Ba_{0.8}Mn_{0.8}Mg_{0.2}O_3$ exhibits the high NO decomposition activity under coexistence of O_2 [17]. $Sm_{0.2}Ce_{0.8}O_{1.9}$ was added in order to enlarge triple phase boundaries (TPB). The performance of the $La_{0.4}Ba_{0.6}Mn_{0.8}Mg_{0.2}$ (LBMM) + $Sm_{0.2}Ce_{0.8}O_{1.9}$ (SDC) composite cathode in the whole system and the phase reaction between LBMM and SDC were also intensely evaluated. The effect of operating temperatures, gas composition on conversion of NO and performance of SOFC are systematically investigated.

2. Experimental

2.1. Powder synthesis

$La_{0.4}Ba_{0.6}Mn_{0.8}Mg_{0.2}O_{3-\delta}$ (LBMM) powders were prepared by combined citric acid and ethylenediaminetetraacetic acid (EDTA) method. Briefly, the admixing stoichiometric amounts of the nitrate salts $La(NO_3)_3$, $Ba(NO_3)_2$, $Mn(CH_3COO)_2$ and $Mg(NO_3)_2$ were introduced into a beaker, and then equal molar of citrate and EDTA respect to total metal ions were added and ammonia was used to adjust the pH value of the aqueous solution around 8. The solution was evaporated by heating on a magnetic heating stirrer with stirring at 90 °C till it became gel. The gel was burnt to produce a solid amorphous precursor. The obtained precursor was calcined at 1000–1200 °C for 8 h under air to achieve a single perovskite phase structure. The obtained catalyst was denoted as LBMM-1000, LBMM-1100 and LBMM-1200, according to the different calcination temperatures.

2.2. Basic characterization

The crystal structure, lattice parameters and crystallite sizes of LBMM were determined by X-ray diffraction (XRD, Bruker D8

ADVANCE, Germany) using Cu $K\alpha$ radiation ($\lambda = 0.15406$ nm) at room temperature in the 2θ ranging from 20° to 80°. The crystalline phase was assigned by using a powder diffraction file database. Peak refinements were performed by using the commercially available software Jade 5.0.

The micromorphology of the catalysts were examined on a JEOL JEM-2100 transmission electron microscope (TEM), samples were deposited on a copper mesh by means of dip coating.

Temperature-programmed desorption (TPD) was carried out on automated chemisorption analyzer (Quantachrome Instruments). About 100 mg of sample was used. After O_2 saturation in 1 h, the gas was switched to He for 0.5 h. Subsequently, TPD was performed by ramping the temperature at 10 °C min^{-1} to 700 °C in He (70 mL min^{-1}). Desorption of O_2 was detected by a thermal conductivity detector (TCD).

The DRIFTS spectra were acquired using an in situ DRIFTS cell equipped with a gas flow system. DRIFTS measurements were performed with Nicolet iZ10 FTIR spectrometers at 4 cm^{-1} resolution with 32 co-added scans. In the DRIFTS cell, the catalyst was pretreated at 400 °C in He. After the background spectrum was recorded with the flowing of He and was subtracted, the sample was exposed to 1000 ppm NO and followed by exposed to 1000 ppm NO + 5% O_2 and the DRIFTS spectra were recorded.

2.3. Chemical stability

The samples LBMM–SDC (mixed with the weight ratio of 80:20) were examined with X-ray diffraction for phase composition.

The chemical stability of the sintered LBMM and LBMM–SDC samples in carbon dioxide atmosphere was studied up to 800 °C in a tube furnace for 2 h in CO_2 environment. The residue was cooled to room temperature (RT). The phase composition of the residue was identified by XRD.

To study the stability of LBMM and LBMM–SDC in boiling water, the powder sample was also heated in boiling water for 2 h, dried at RT, and XRD pattern of residue was also recorded.

2.4. Fuel cell measurements

For cell test, the electrolyte $Ce_{0.8}Sm_{0.2}O_{1.9}$ (SDC) was prepared by EDTA-Citric combustion method in the previously report. Anode-support complete cells with the SDC electrolyte were prepared using a co-pressing technique. The anode powders were consisting of 60 wt.% NiO and 40 wt.% SDC. Than the anode and electrolyte were pressed into a pellet with the thickness of 0.8 mm and diameter of 30 mm. the pellet was sintered at 1400 °C for 8 h to achieve densification. The cathode layer was deposited by brush painting cathode ink, which consists of LBMM, SDC (LBMM:SDC = 8:2), glycerol, ethylene glycol and isopropyl alcohol by the ball mill at 45 Hz for 24 h. Then the LBMM–SDC colloidal suspension was spray deposited onto the electrolyte surfaces of the sintered pellets. The membrane electrode assemblies (MEAs) (cell with configuration: anode/electrolyte/cathode: Ni-SDC/SDC/LBMM–SDC) fired at 1000 °C for 4 h to form the cell. Ag mesh was pressed onto the electrodes by spring loading, used as a current collector for both the cathode and anode. Anode chamber of the MEAs was 10% H_2–N_2 with the flow rate 60 mL min^{-1}, while cathode with 5% or 1% NO–Ar with the flow rate 100 mL min^{-1}. The inlet flow rates of both anode and cathode gases were controlled using mass flow controllers. The fuel cell tests were performed in a furnace having a coaxial two-tube (inlet and outlet) set-up at each face of the cell sealed by ceramic sealant at temperatures 600 °C.

Symmetric cells with the configuration of electrode |SDC| electrode were applied for the impedance studies. The electrochemical effects were measured via electrochemical impedance spectrum measurement by an electrochemical work station (ParSTAT4000).

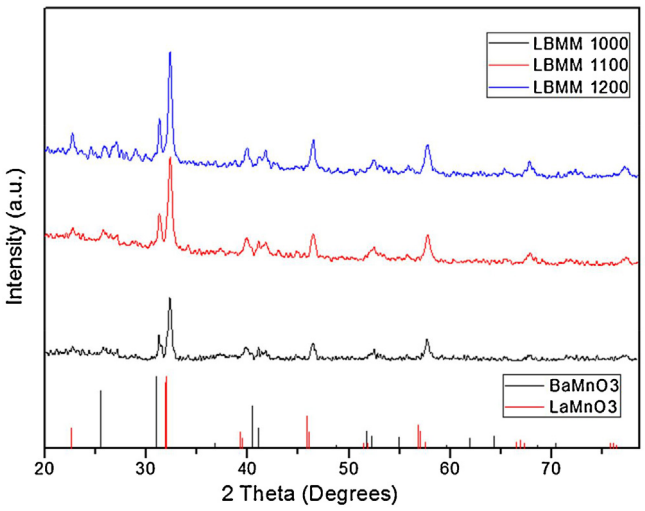

Fig. 2. XRD patterns of $La_{0.4}Ba_{0.6}Mn_{0.8}Mg_{0.2}O_{3-\delta}$ powders calcined at different temperature.

3. Results and discussion

3.1. Structure and surface analysis of the material

Fig. 2 displayed the X-ray diffraction (XRD) patterns of $La_{0.4}Ba_{0.6}Mn_{0.8}Mg_{0.2}O_{3-\delta}$ calcined at different temperatures. It can be seen that the powers are well crystallized at 1000 °C. The effects of La amount at the Ba site on NO decomposition were meticulous studied by Ishihara [17,18]. $BaMnO_3$ is the main phase at low La content; otherwise, $LaMnO_3$ is the main phase. The amount of Mg in here is 0.2. Due to the formation of impurity phase starts at 0.25 and it becomes significant with increasing the amount of Mg higher than 0.2 [17]. All the main diffraction peaks can be assigned to them. Therefore, the doped Mg successfully substitutes the lattice position of B-site (Mn) in $La_{0.4}Ba_{0.6}MnO_3$. The average crystallite size calculated is 19 nm from Scherrer's formula as

$$D = \frac{K\lambda}{\beta\cos\theta} \quad (1)$$

where D is the particle size, K is the Scherrer constant, λ is the X-ray radiation wavelength, θ is the angle of XRD peak, and β is the full width at half maxima (FWHM). After correction the formula is as follows:

$$D = \frac{0.89 \times 0.15406}{(\beta - 0.09/180) \times \pi \times \cos\theta} \quad (2)$$

The reaction between LBMM and SDC at various firing temperatures were investigated. LBMM and SDC were mechanically mixed at the weight ratio of 80:20 with ball miler employing zirconium oxide as the grinding ball and alcohol as the solvent and then calcined in air for 8 h. 1000 °C calcined LBMM and 1000 °C calcined SDC from an EDTA-citrate complexing process were applied as the raw materials for this research. Fig. 3 shows the X-ray diffraction patterns of the LBMM + SDC composite oxide calcined at different temperatures. Before the calcination temperature was elevated to 1100 °C, the LBMM + SDC showed similar diffraction patterns to the raw materials. When the temperature was elevated to 1100 °C, the perovskite phase and fluorite phase completely changed, suggesting there were phase reaction between LBMM and SDC.

Sol–gel synthesis based on EDTA-citrate complexing process was used to examine the products of LBMM and SDC. $La(NO_3)_3$,

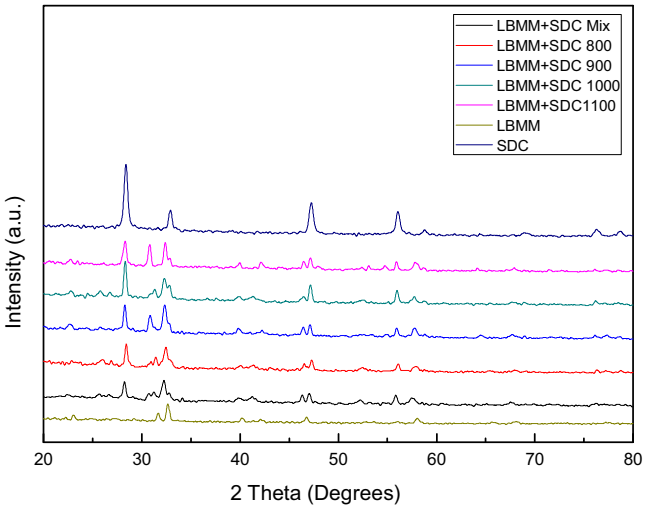

Fig. 3. XRD patterns of LBMM + SDC after calcined in air at various temperature for 10 h.

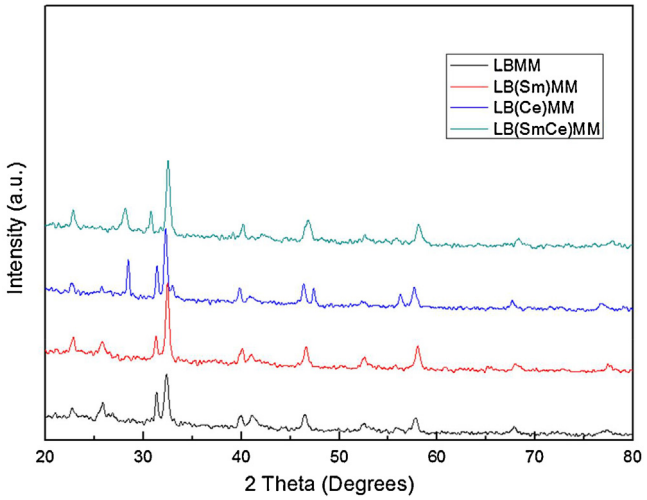

Fig. 4. XRD patterns of LBMM, LB(Sm)MM, LB(Ce)MM, LB(SmCe)MM.

$Ba(NO_3)_2$, $Mn(NO_3)_2$, $Mg(NO_3)_2$, $Sm(NO_3)_3$ and $Ce(NO_3)_3$ according to the stoichiometry of LBMM + SDC (80:20 in weight ratio) were mixed in the solution and further calcined at 1100 °C for 8 h. The obtained products reflect the most stable production of the solid–state reaction between LBMM and SDC. It is well known that Sm and Ce can both dope into the A-site and B-site of the perovskite. However, Sm^{3+}(0.958 Å),Ce^{3+} (1.01 Å) and Ce^{4+}(0.87 Å) have smaller ionic radii than La^{3+} (1.36 Å) and Ba^{2+} (1.61 Å), and the doping into A-site of LBMM would result in the shrinking of the lattice, but they have larger ionic radii than Mn^{2+} (HS-0.83 Å), Mn^{3+} (HS-0.645 Å), Mn^{4+} (HS-0.53 Å) and Mg^{2+}(0.72 Å). The doping of Ce or Sm into B-site would result in the expansion of the lattice. Therefore, Sm and Ce were likely incorporated into the A-site of LBMM. However, there is a strong peak of CeO_2 from the XRD of $(La_{0.4}Ba_{0.6})_{0.8}Ce_{0.2}Mn_{0.8}Mg_{0.2}O_{3-\delta}$ and $(La_{0.4}Ba_{0.6})_{0.8}(Sm_{0.2}Ce_{0.8})_{0.2}Mn_{0.8}Mg_{0.2}O_{3-\delta}$ in Fig. 4. Its means Ce cannot be doping in LBMM at the 1100 °C. It's demonstrated that the phase reaction between LBMM and SDC was closely related with the firing temperatures.

Fig. 5 shows the TEM and HR-TEM of LBMM (calcined at 1000 °C) and LBMM + SDC (8:2 calcined at 1000 °C). The TEM images of the prepared LBMM and LBMM–SDC were shown in Fig. 5a and b. Obviously, the particles of LBMM + SDC were clustered. The average crystallite size Of LBMM was 10–20 nm. The results were in accord with the results of XRD. The images of the sample a and b showed that the surface was smooth and some pores could be found, which indicated that the specific surface area of LBMM was high relatively.

HR-TEM was performed to ascertain the crystallite growth and morphology of the Sample. For all the samples, the lattice fringes

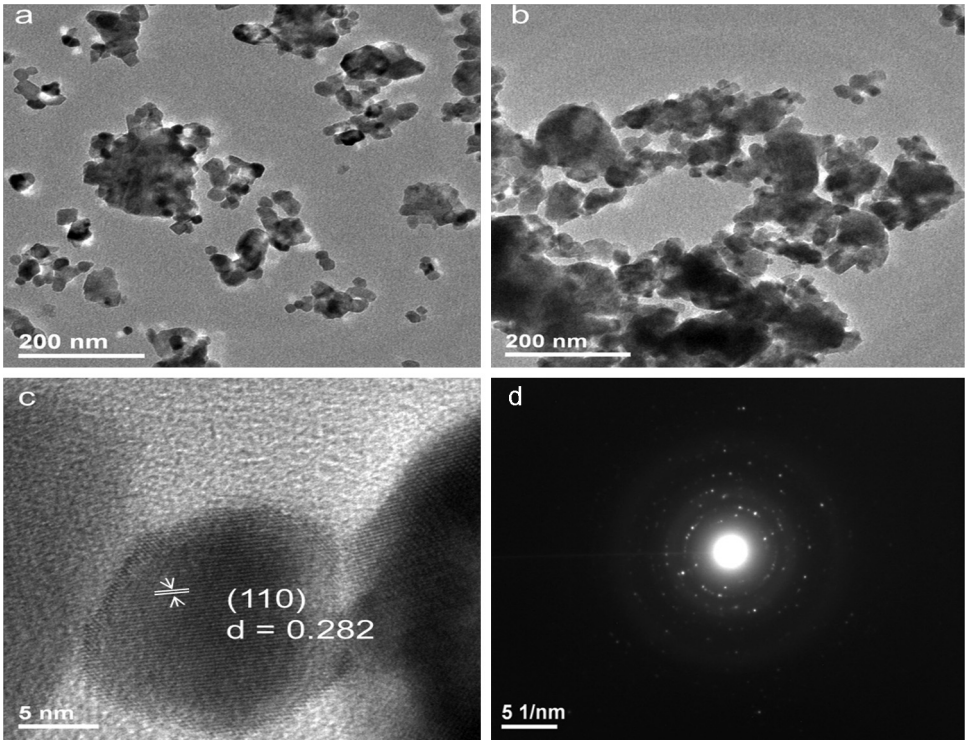

Fig. 5. (a) TEM image of LBMM (b) TEM image of LBMM–SDC (c) HRTEM image of LBMM (d) electron diffraction patterns of LBMM.

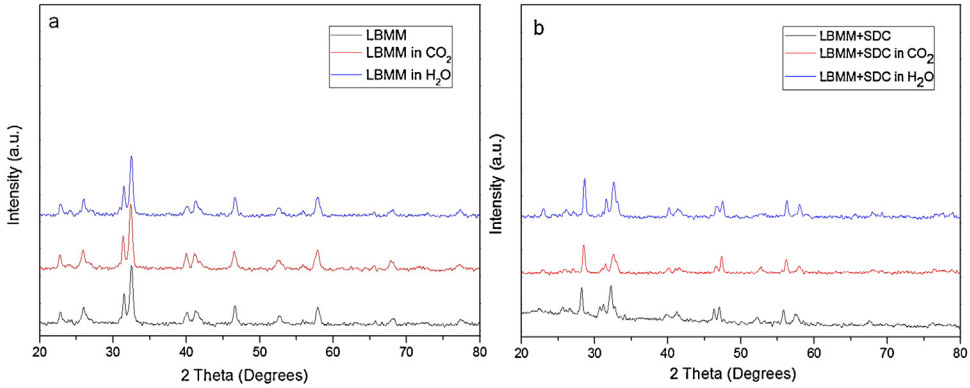

Fig. 6. The XRD patterns of LBMM, LBMM–SDC powders after chemical stability test.

were observed as about 0.282 nm periodically, which was compatible with the distance between the (1 1 0) plane of LBMM. The results were also in accord with the results of XRD.

3.2. Chemical stability

To evaluate the chemical stability against CO_2 and water vapor, LBMM powders, LBMM–SDC powders and dense pellets were treated in CO_2 atmospheres, even in boiling water. Fig. 6a and b shows the XRD patterns of LBMM, LBMM–SDC powders after chemical stability test. It can be seen, the pattern of LBMM, LBMM–SDC powders remains unchanged after exposed to CO_2 at 800 °C for 2 h and no other phases were formed when the LBMM, LBMM–SDC was treated in boiling water for 2 h. The results suggest that with the doping of La, LBMM is indeed much more chemically stable than $BaMnO_3$-based perovskite, which can be easily corroded by CO_2 or water vapor.

Fig. 7 shows the O_2-TPD profiles of LBMM and LBMM–SDC. The generation of oxygen vacancies is an important parameter for determining the oxygen reduction reaction (ORR) activity of a catalyst. Two desorption peak were observed for all the samples, one between 200 °C and 400 °C and the other between 550 °C and 850 °C. Generally, oxygen defects are formed when a perovskite is heated at high temperature. Two different types of oxygen are known for perovskote, α-oxygen (suprafacial oxygen) desorbed at relatively lower temperature and β oxygen (interfacial oxygen), which is desorbed at high temperature. The α and β oxygen usually belong to surface and bulk, respectively. As indicated in Fig. 7, with the incorporation of SDC, the desorption peak in the low temperature and high temperature peak were shifted to higher temperature and became further stronger. It also showed a very good repeatability of O_2-TPD pattern of LBMM and LBMM + SDC, which demonstrated good reversibility of oxygen adsorption and desorption ability of those material.

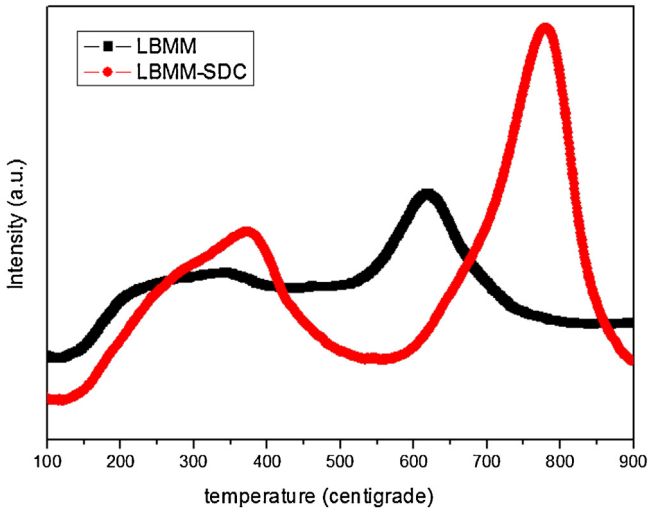

Fig. 7. O_2-TPD profiles of LBMM and LBMM–SDC.

3.3. Electrochemical characterization

The electrocatalytic activity of LBMM and LBMM–SDC for oxygen reduction on electrolyte SDC was first investigated by symmetric cell test. Fig. 8a–d shows typical EIS of LBMM|SDC|LBMM and LBMM–SDC|SDC|LBMM–SDC in air or in 5% NO-containing atmosphere between 550 and 800 °C, respectively. The performance of ac impedance shows disciplinary numerical results. It is observed that no matter in air or in NO atmosphere, the resistance quickly reduced with the rise of temperature. The impedance can be greatly influenced by different atmosphere even under the same temperature. Ohm resistance and polarization resistance in NO are greater than the same impedance under the temperature in air. The existence of oxygen vacancy in this material could adsorb NO in the environment, which would cause the energy level of a catalyst changed. This is one of the reasons for ohm impedance increases. As compared to O_2, the transfer of oxygen and nitrogen in the process of NO direct decomposition under the action of catalyst, the existence of those chemical reactions would also affect the ohm impedance. It is also observed that the composite electrodes with SDC increased the electrochemical activity. It generally have lower resistance values than the LBMM. As for the increase polarization impedance values of LBMM or LBMM–SDC appear in NO containing environment. The NO decomposition compared with the oxygen reduction is divided into four steps and the control speed of step requires higher activation energy [30]. Furthermore the polarization resistance also depended on the amount of oxygen vacancy [31]. The electrodes with LBMM have much higher polarization resistance in air and NO containing atmosphere than the ones based on LBMM–SDC.

3.4. Cell performance

To study the effect of the gas composition on the SOFC performance, especially the different concentrations of NO and the addition of oxygen in cathode chamber, we fed four types of gas compositions to the cathode with 5% and 10% of hydrogen to the anode: Gas 1. 1000 ppm NO; 2. 5% NO; 3. 1000 ppm NO + 5% O_2; 4. 5% NO + 5% O_2 (all carried by Ar). The voltage-current and power-current characteristics of the cells at 600 °C was shown in Fig. 9. When only NO was fed to the cathode without the addition of oxygen, the open circuit voltage (OCV) and peak powder density

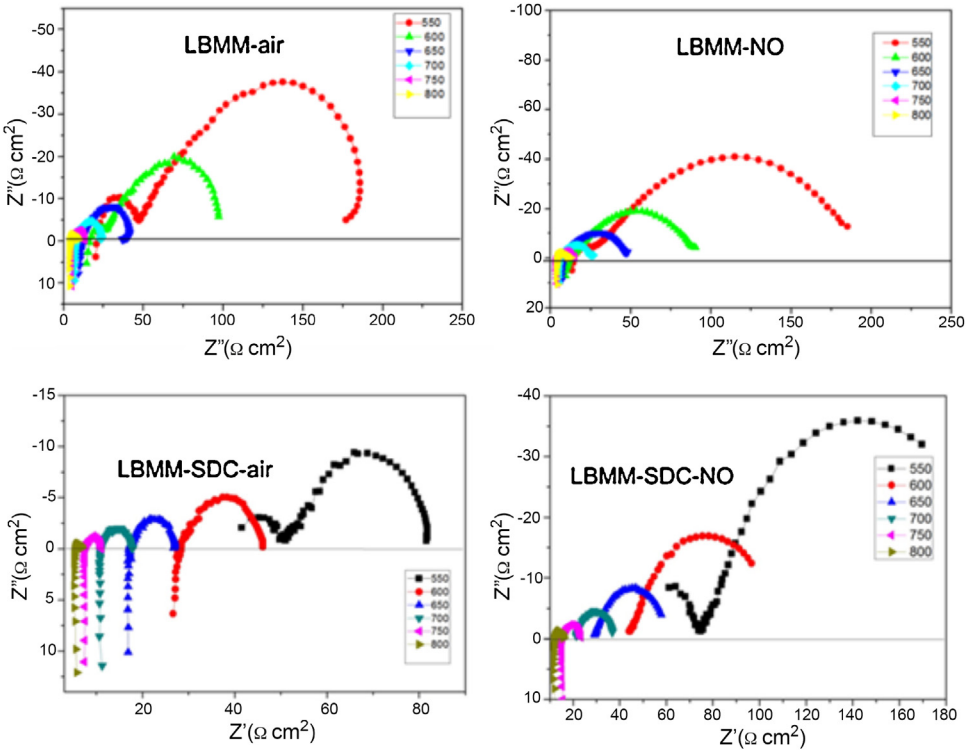

Fig. 8. The Nyquist impedance curve for the symmetric cell LBMM|SDC|LBMM and LBMM–SDC|SDC|LBMM–SDC measured at different temperature.

of the cell increased significantly with the concentration of NO. This suggested that more oxygen could be generated coupled with the decomposition of NO, which increased the chemical potential between the both sides of the cell and allowed more oxygen to transport through the electrolyte, thus increased performance. For example, when 1000 ppm and 5% NO and was fed to the cathode, the OCV are 0.42 V and 0.55 V and the peak power density are 1.6 and 2.4 mW cm^{-2}, respectively. When 5% oxygen was added in the cathode gas, OCV and peak power density can be further enhanced with a maximum peak power density of 11.6 and 25.3 W cm^{-2}. Also, the addition of oxygen are more critical to the SOFC performance than NO, although it is demonstrated to be detrimental to NO conversion, as shown in Fig. 10. Note that the level of hydrogen has a significant effect on OCV and peak power density in present study. For example, When cathode gas is fixed 5% NO, OCV and peak power density of the cell increased from 0.55 V to 0.66 V when the concentration of hydrogen increased from 5% to 10%. Fig. 10 shows the comparison of catalytic performance at various temperatures (from 200 °C to 600 °C) over the LBMM–SDC catalysts supported on SOFC. The temperature of the system played an important role on the NO conversion. The conversion rate of the NO_x was increased gradually with the temperature. For NO decomposition under anaerobic conditions, the activity was gradually reach the peak date about 98% to 99% during 500 to 600 °C. Compared to the former work reported [18], the temperature is significantly reduced.

Under oxygen condition, it reached 83.6% of the 400–450 °C, then drop rapidly. And keep in a certain range about 44%. Actually in here NO content constitute a sizable, there was greater concentration of NO_2 examined by a Ecom-JZKN flue gas analyzer (Germany). In order to further understand the catalytic mechanism

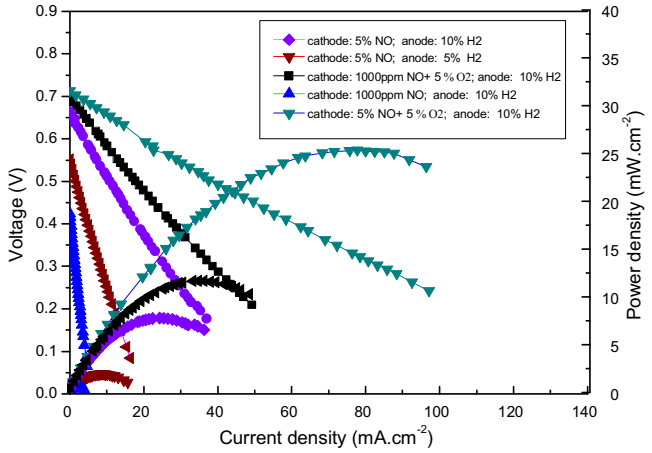

Fig. 9. I–V and I–P curves for the complete cell based on Ni-SDC|SDC|LBMM working under different No concentration (balanced by Ar).

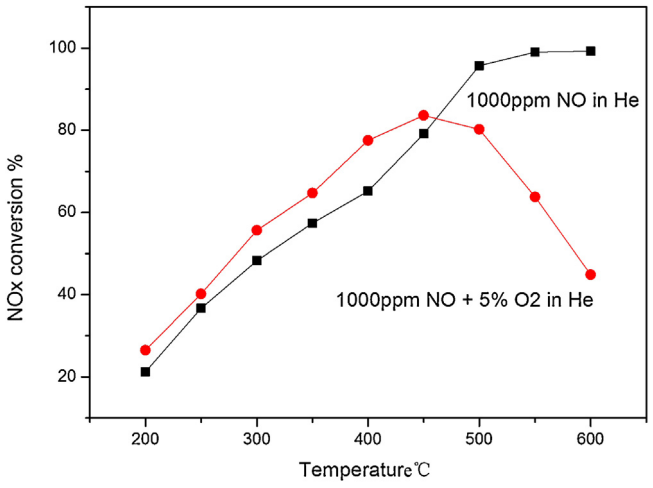

Fig. 10. NO_x conversion of SOFC with different atmosphere in cathode.

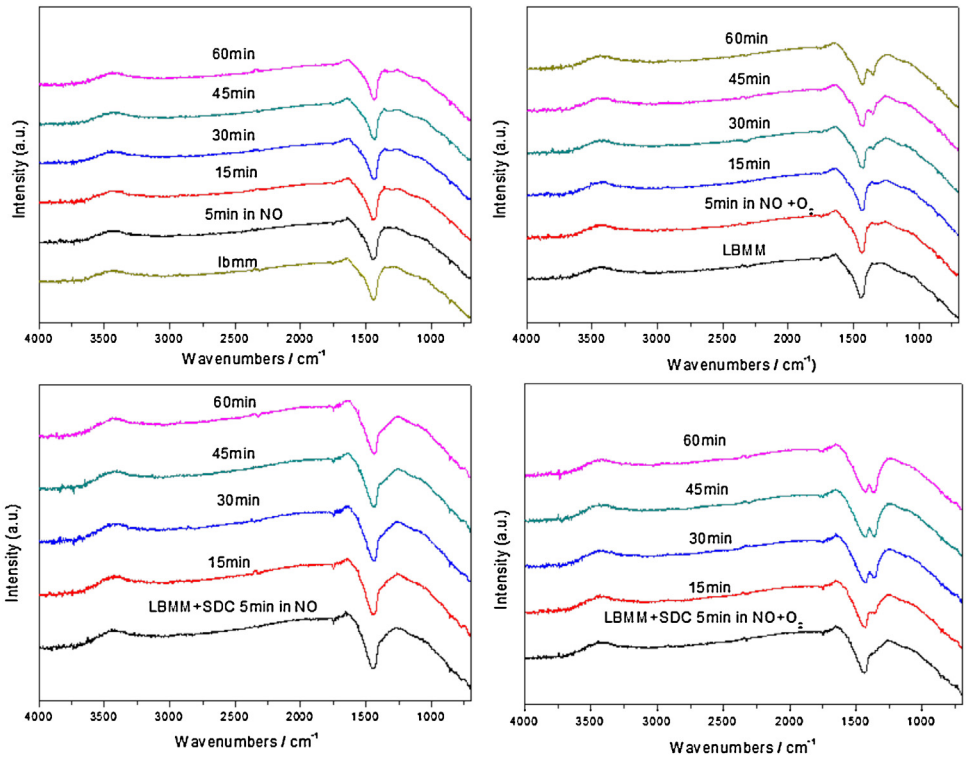

Fig. 11. DRIFTS spectra of LBMM and LBMM–SDC under exposure to 1000 ppm NO at 400 °C for various time and followed by exposure to 1000 ppm NO + 5% O_2 for various time.

under anaerobic and aerobic conditions. The In-situ DRIFTS measurements were employed.

Fig. 11 showed the spectra after the introduction of 1000 ppm NO at 400 °C and followed 5% O_2 was introduced. There are no new bonds appearances with the time rise in LBMM. For LBMM–SDC in NO, there are only the weak bands at 1740–1800 cm^{-1} could be detected. According to the literature [35,36], the bands could be assigned to the weak NO adsorption, which was in the form of NO^+. It can be observed that the adsorbed NO were limited over LBMM. However, LBMM–SDC can adsorb more NO actually which is helpful for NO decomposition. This observation is consistent with the mechanism of NO decomposition on perovskite oxides in Fig. 11 While O_2 supply was switched on, some new bands formed, such as the bands at 1347.5–1355.7 cm^{-1}. The surface of tested catalysts was covered by monodentate nitrate (1350 cm^{-1}) [37–39]. Moreover, the bands grew with the increasing of time, and the intensities reached the strongest after the NO feeding for 15 min. The formed nitrates were clearly appeared on LBMM and LBMM–SDC. It can be draw the conclusion that NO decomposition happened after adsorb in the absence of oxygen environment. However, when under oxygen environments, the adsorption NO in the catalytic surface is oxidized to nitrate, At above 450 °C, the stored nitrate became unstable and decomposed, resulting in the sharp decrease of, the stored nitrate became unstable and decomposed, resulting in the sharp decrease of NO_x conversion rate in Fig. 9. The existence of nitrate not only maintains the NO_x conversion rate at a certain amount below 450 °C, but also the main factors affecting the electrochemical properties.

Based on the cell performance, NO conversion and in situ DRIFT, An important implication is unlike the traditional catalyst for NO decomposition in fixed bed, the electrochemical decomposition of NO coupled with a SOFC have capability to reduce the temperature for the decomposition. This is because the reaction of the NO decomposition directly produced N_2 and O_2, and O_2 can be used as oxidant for an reduced temperature SOFC, which is a driving force to push the decomposition reaction forward. It is also confirmed by the in situ DRIFT. On the other hand, when oxygen was mixed with NO and fed to the cathode, the system became more complicated and it tends to be a competition between oxygen and NO, which could enhance SOFC performance while reducing the NO conversion. It is also confirmed by in situ DRIFT. The presence of nitrate implies NO can be oxidized into NO_2 and NO_3^- rather than N_2 and O_2.

4. Conclusions

A new electrochemical system, combining the direct decomposition of No_x with an electric gene ration process through an intermediate temperature SOFC, was studied. The conventional material for catalysis of NO decomposition, LBMM with grain size of ~20 nm was synthesized and investigated as a cathode material for IT-SOFC. The reduced temperature for NO decomposition and the operating of SOFCs were demonstrated with the anode-support SOFC using LBMM–SDC composite as cathode. The NO_x decomposition is complete above 550 °C when there is only NO fed in cathode. When Ar containing 5% No and the additional 5% oxygen was fed to the cathode and H_2 was used as the fuel, the peak power density of SOFC is 25.3 mW cm^{-2} at 600 °C. Present results suggested that SOFC can be used as an effective catalytic device for NO_x decomposition at reduced temperatures while generating the power.

Acknowledgments

This work was financially supported by the National Natural Science Foundation of China (U1162119 and 51078185), the research fund of Key Laboratory for Advanced Technology in Environmental Protection of Jiangsu Province (AE201001), Research Fund for the Doctoral Program of Higher Education of China (20113219110009), Industry-Academia Cooperation Innovation

Fund Projects of Jiangsu Province (BY2012025) and Scientific Research Project of Environmental Protection Department of Jiangsu Province (201112).

References

[1] W.J. Hong, S. Iwamoto, M. Inoue, Catal. Today 164 (2011) 489.
[2] F.E. Lopez-Suarez, M.J. Illan-Gomez, A. Bueno-Lopez, J.A. Anderson, Appl. Catal., B: Environ. 104 (2011) 261.
[3] H. Xian, X.W. Zhang, X.G. Li, H.H. Zou, M. Meng, Z.Q. Zou, L.H. Guo, N. Tsubaki, Catal. Today 158 (2010) 215.
[4] K.K. Hansen, Appl. Catal., B: Environ. 100 (2010) 427.
[5] C. Márquez-Alvarez, I. Rodríguez-Ramos, A. Guerrero-Ruiz, G.L. Haller, M. Fernández-García, J. Am. Chem. Soc. 119 (1997) 2905.
[6] S. Zhang, X. Liu, Q. Zhong, Y. Yao, Catal. Commun. 25 (2012) 7.
[7] J. Zhang, S. Zhang, W. Cai, Q. Zhong, Appl. Surf. Sci. 268 (2013) 535.
[8] M. Inagaki, T. Imai, T. Yoshikawa, B. Tryba, Appl. Catal., B: Environ. 51 (2004) 247.
[9] H. Yamashita, Y. Ichihashi, S.G. Zhang, Y. Matsumura, Y. Souma, T. Tatsumi, M. Anpo, Appl. Surf. Sci. 121 (1997) 305.
[10] R. Jiang, S. Huang, A.T. Chow, J. Yang, J. Hazard. Mater. 164 (2009) 432.
[11] K.K. Hansen, J. Electrochem. Soc. 157 (2010) P79.
[12] K. Kammer, Appl. Catal., B: Environ. 58 (2005) 33–39.
[13] M.A. Peralta, B.S. Sanchez, M.A. Ulla, C.A. Querini, Appl. Catal., A: Gen. 393 (2011) 184.
[14] W.J. Hong, M. Ueda, S. Iwamoto, S. Hosokawa, K. Wada, M. Inoue, Catal. Lett. 142 (2012) 32.
[15] J.J. Zhu, A. Thomas, Appl. Catal., B: Environ. 92 (2009) 225.
[16] J.J. Zhu, X.G. Yang, X.L. Xu, K.M. Wei, J. Phys. Chem. C 113 (2009) 16838.
[17] H. Iwakuni, Y. Shinmyou, H. Yano, H. Matsumoto, T. Ishihara, Appl. Catal., B: Environ. 74 (2007) 299.
[18] T. Ishihara, M. Ando, K. Sada, K. Takiishi, K. Yamada, H. Nishiguchi, Y. Takita, J. Catal. 220 (2003) 104.
[19] J.J. Zhu, D.H. Xiao, J. Li, X.G. Yang, Y. Wu, J. Mol. Catal. A: Chem. 234 (2005) 99.
[20] W.J. Hong, S. Iwamoto, S. Hosokawa, K. Wada, H. Kanai, M. Inoue, J. Catal. 277 (2011) 208.
[21] J.J. Zhu, D.H. Xiao, J. Li, X.G. Yang, K.M. Wei, Catal. Commun. 7 (2006) 432.
[22] N. Imanaka, T. Masui, Appl. Catal., A: Gen. 431 (2012) 1.
[23] S. Pancharatnam, J. Electrochem. Soc. 122 (1975) 869.
[24] K. Kammer, E.M. Skou, Solid State Ionics 176 (2005) 915.
[25] T.J. Huang, I.C. Hsiao, Chem. Eng. J. 165 (2010) 234.
[26] T.-J. Huang, C.-Y. Wu, D.-Y. Chiang, C.-C. Yu, Appl. Catal., A: Gen. 445 (2012) 153.
[27] T.-J. Huang, C.-Y. Wu, S.-H. Hsu, C.-C. Wu, Appl. Catal., B: Environ. 110 (2011) 164.
[28] H.Q. Jiang, H.H. Wang, F.Y. Liang, S. Werth, T. Schiestel, J. Caro, Angew. Chem. Int. Ed. 48 (2009) 2983.
[29] H.Q. Jiang, L. Xing, O. Czuprat, H.H. Wang, S. Schirrmeister, T. Schiestel, J. Caro, Chem. Commun. 21 (2009) 6738.
[30] N. Imanaka, T. Masui, Appl. Catal., A: Gen. 1 (2012) 431.
[31] R.M.L. Werchmeister, K.K. Hansen, M. Mogensen, J. Electrochem. Soc. 157 (2010) P107.
[35] Y.L. Wang, C.Z. Ge, L. Zhan, C. Li, W.M. Qiao, L.C. Ling, Ind. Eng. Chem. Res. 51 (2012) 11667.
[36] P. Pietrzyk, K. Podolska, Z. Sojka, J. Phys. Chem. C 115 (2011) 13008.
[37] F. Liu, H. He, J. Phys. Chem. C 114 (2010) 16929.
[38] L.Q. Nguyen, C. Salim, H. Hinode, Appl. Catal., B: Environ. 96 (2010) 299.
[39] G. Jing, J. Li, D. Yang, J. Hao, Appl. Catal., B: Environ. 91 (2009) 123.